**Remote Sensing Letters**
September 2022, Volume 13 Issue 9 Pages 946-957
https://doi.org/10.1080/2150704X.2022.2112107
https://archimer.ifremer.fr/doc/00788/90040/

**Archimer**
https://archimer.ifremer.fr

# Two-dimensional structure functions for characterizing convective rolls in the marine atmospheric boundary layer from Sentinel-1 SAR images

Granero Belinchon Carlos [1, *], Roux Stéphane G. [2], Garnier Nicolas B. [2], Tandeo Pierre [1], Chapron Bertrand [3], Mouche Alexis [3]

[1] Mathematical and Electrical Engineering Department, IMT Atlantique, Lab-STICC, UMR CNRS 6285, Brest, France
[2] Laboratoire de Physique, Univ Lyon, Ens de Lyon, CNRS UMR 5672, Lyon, France
[3] Laboratoire d'Océanographie Physique et Spatiale, Ifremer, Univ. Brest, CNRS, IRD, IUEM, Plouzané, France

* Corresponding author : Carlos Granero Belinchon, email address : carlos.granero-belinchon@imt-atlantique.fr

**Abstract :**

We study the shape of convective rolls in the Marine Atmospheric Boundary Layer from Synthetic Aperture Radar images of the ocean. We propose a multiscale analysis with structure functions which allow an easy generalization to analyse high-order statistics and so to finely describe the shape of the rolls. The two main results are 1) second-order structure function characterizes the wavelength and direction of rolls just like correlation or power spectrum do, 2) high-order statistics can be studied with skewness and flatness which characterize the asymmetry and intermittency of rolls, respectively. This is the first time that the asymmetry and intermittency of rolls are shown from radar images of the ocean surface.

**Keywords** : Multiscale analysis, High-order statistics, Structure functions, Convective rolls, Ocean-Atmosphere boundary layer

Please note that this is an author-produced PDF of an article accepted for publication following peer review. The definitive publisher-authenticated version is available on the publisher Web site.

## 1. Introduction

Depending on the surface layer stratification, rolls approximatively aligned with the mean flow can develop in the Marine Atmospheric Boundary Layer (MABL) into Organised Large Eddies (OLE). Although, this secondary circulation plays a key role in turbulent heat and momentum fluxes (Zhang et al. 2008), MABL fluxes parameterization and modelling is still an active field of research for both the numerical models (Sandu et al. 2013) and Large Eddies simutations (Saggiorato et al. 2020). One of the reasons is certainly that ground truth for collocated wind, temperature and humidity profile observations and for documenting OLE characteristics in open ocean are rare. As summarized by (Etling and Brown 1993), the main known characteristics are the following: vertical extent: 1-2 km, wavelength: 2-20 km, aspect ratio: 2-15, downstream extent: 10-1000 km, orientation of roll axis to mean wind direction:

CONTACT Carlos Granero-Belinchon. Email: carlos.granero-belinchon@imt-atlantique.fr

-20° to +30°; and lifetime: 1-72 h. Yet, more advanced information such as their frequency of occurrence, strength or formation remains to be documented. For a more complete review on OLE from the observational, theoretical and numerical point of view, the reader can refer to review papers from (Etling and Brown 1993) and (Young et al. 2002).

C-Band high-resolution radar (or SAR for synthetic aperture radar) is the only spaceborne instrument able to probe at very high spatial resolution ocean sea surface day and night, regardless of the cloud coverage, with pixel resolution of few meters in swaths of several hundred kilometers. At C-band (about 5 cm), the backscattered signal from the ocean is primary sensitive to capillary and small gravity ocean surface waves which are very sensitive to the local surface stress allowing for the SAR to trace the horizontal wind field convergence and divergence areas in between the rolls. As a consequence, several studies have been conducted to report on the rolls signature on SAR images (Alpers and Brümmer 1994; Sikora and Ufermann 2004) and document the spatial evolution of convection for particular events such as strong cold outbreak interacting with the Gulf Stream north wall (Babin, Sikora, and Winstead 2003). Most of them focused on coastal areas where large images with a width of several hundreds of kilometers were acquired with previous SAR missions Envisat and Radarsat. But, very few take benefit of the acquisition mode used in open ocean : the so-called Wave Mode (WV). In fact, the only studies based on wave mode have been published by (Wang et al. 2020) for OLE detection and (Wang et al. 2019) for OLE documentation (orientation and wind speed modulation of $\pm$ 7 m $s^{-1}$). In particular, these two recent studies rely on the new capabilities of Sentinel-1 European SAR mission that provides images of 20 km $\times$ 20 km over open ocean whereas the former European SAR (Envisat) was only able to provide scenes of 8 km $\times$ 10 km, much less adapted to the OLE wavelength. Moreover, WV acquisition mode have the highest resolution: about 5 m.

Until now, previous works only used second order statistics to characterize wavelength and direction (with an ambiguity of $\pi$ rad) of convective rolls directly from radar imagery of the atmosphere (Lohou, Druilhet, and Campistron 1998) or from SAR imagery of the ocean (Wang et al. 2019, 2020). However, higher order statistics have been already used to characterize turbulence in 1-dimensional signals of wind velocity in the MABL (Atta and Chen 1970). Thus, we propose here to use higher order statistics to characterize more subtly the shape of convective rolls. To do so, we compute the 2-dimensional skewness $\mathcal{S}$ and flatness $\mathcal{F}$ of spatial increments and examine their evolutions across length-scales (Frisch 1995), which allows us to describe the asymmetry and intermittency of convective rolls. On the one hand, intermittency characterizations of roll structures can improve the description of turbulence in the MABL needed for weather forecasting and climate modeling (Sikora and Ufermann 2004). More generally, this work paves the way for further analysis of these new SAR-derived parameters with respect to the MABL characteristics. On the other hand, the asymmetry characterization of rolls overcomes the ambiguity of $\pi$ rad in the rolls direction determination provided by only second-order statistics (Wang et al. 2019, 2020). This new information could help for getting an independent estimate of the wind direction from the analysis of SAR image texture. This is the first time that such an analysis is performed on SAR images.

## 2. Methods

### 2.1. *Two-dimensional direction-dependent structure functions*

The $n$th order structure function $S_n$ of a two-dimensional field $F(x, y)$ can be defined as:

$$S_n^{l_x,l_y}(F) = \langle (F(r_x + l_x, r_y + l_y) - F(r_x, r_y))^n \rangle \tag{1}$$

where $(r_x, r_y)$ denotes a spatial position, and so $l_x$ and $l_y$ are the spatial separation distances between the two samples of $F$ and along each dimension of the field. We then note $\delta_{l_x,l_y}F = F(r_x + l_x, r_y + l_y) - F(r_x, r_y)$, the spatial increment of the two-dimensional field.

In this paper we focus on $S_2^{l_x,l_y}$, $S_3^{l_x,l_y}$ and $S_4^{l_x,l_y}$ that provide respectively a characterization of the variance, asymmetry and tails prominence of the statistical distribution of the increments of the field at scales $(l_x, l_y)$. To avoid the impact of $S_2^{l_x,l_y}$ variations on the characterization of $S_3^{l_x,l_y}$ and $S_4^{l_x,l_y}$, the skewness $\mathcal{S}$ and flatness $\mathcal{F}$ factors across scales are defined. They correspond to $S_3^{l_x,l_y}$ and $S_4^{l_x,l_y}$ on centered and standardized increments.
If $\mathcal{S} = 0$ then the distribution is symmetrical, while $\mathcal{S} < 0$ implies left-tailed and $\mathcal{S} > 0$ right-tailed distributions. On the other hand, the flatness of a Gaussian distribution is $\mathcal{F} = 3$, while $\mathcal{F} < 3$ means less prominent tails and $\mathcal{F} > 3$ more prominent ones.

From a physical point of view, $S_2^{l_x,l_y}$ characterizes the distribution of energy across scales, while $\mathcal{S}^{l_x,l_y}$ and $\mathcal{F}^{l_x,l_y}$ allow us to describe intermittency which translates into a deformation of the shape of the distribution across scales (Frisch 1995). Thus for example turbulence is characterized by a Gaussian distribution at large scales and an increase, of skewness and flatness when the scale decreases (Kolmogorov 1962; Obukhov 1962; Frisch 1995).

Finally, a change of coordinates from cartesian to polar allows for analysis with respect to direction: $S_2^{l_x,l_y} \rightarrow S_2^{r,\theta}$, $\mathcal{S}^{l_x,l_y} \rightarrow \mathcal{S}^{r,\theta}$ and $\mathcal{F}^{l_x,l_y} \rightarrow \mathcal{F}^{r,\theta}$, with $r$ the radius and $\theta$ the angle dimension.

### 2.2. *Interpretation of structure functions analysis of OLE*

So, second order statistics such as power spectrum, correlation function or $S_2^{l_x,l_y}$, describe the wavelength and direction of convective rolls (Lohou, Druilhet, and Campistron 1998; Wang et al. 2019, 2020) without providing finer information nor on the shape of rolls neither on the evolution of this shape across scales. Thus from (Lohou, Druilhet, and Campistron 1998), the correlation function decreases the fastest along the direction perpendicular to the rolls $\theta_\perp$. Moreover, along this direction the correlation length, measured as the distance to the first minimum, indicates the wavelength of the rolls. On the other hand from (Wang et al. 2019, 2020), peaks of energy appear in the 2-dimensional power spectrum and the most energetic peaks indicate the wavelength and direction of rolls. Since power spectrum and correlation (equivalently $S_2^{l_x,l_y}$) are simply related by the Fourier transform, both methodologies are equivalent. These second order statistics are frequently used in the characterization of ocean surface from remote sensing images (Tandeo et al. 2014).

Contrary to second-order statistics, high order ones such as $\mathcal{S}^{l_x,l_y}$ and $\mathcal{F}^{l_x,l_y}$ characterize the shape of the rolls and its finer changes across scales. More precisely, non-zero values of $\mathcal{S}^{l_x,l_y}$ illustrate an asymmetry of the shape of the rolls along the direction

pointed out by the couple $(l_x, l_y)$. Indeed, $\mathcal{S}^{l_x,l_y}$ characterizes the asymmetry of the distribution of the increments of size $(l_x, l_y)$, and so, characterizes the differences between rises and falls of the field along this direction and at this scale, see figure 1. We interpret low intensity areas of SAR fields as areas occupied by the rolls, while high intensity areas are interpreted as areas between rolls. Thus, $\mathcal{S}^{l_x,l_y} \neq 0$ along $\theta_\perp$ implies that we enter and leave rolls in a different way (more or less smoothly/sharply) pointing out an asymmetry, see figure 1.

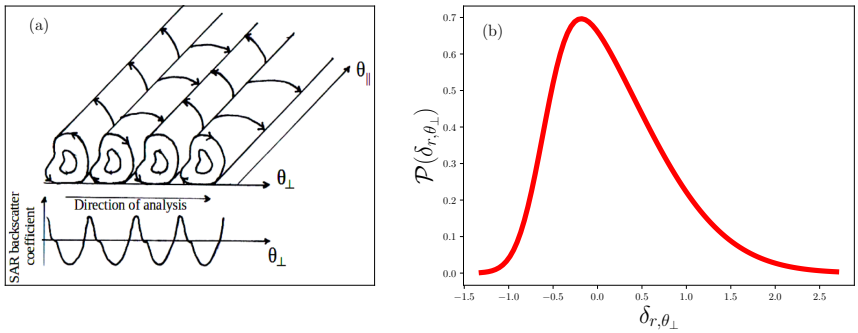


**Figure 1.** a) Outline of asymmetrical convective rolls and their SAR imprint. The direction of analysis corresponding to $\theta_\perp$ is indicated by the *direction of analysis* arrow. b) Schematic distribution of the increments $(\delta_{r,\theta_\perp})$ of the SAR backscatter coefficient at a given scale $r$ smaller than the rolls wavelength and along the direction $(\theta_\perp)$ indicated by the *direction of analysis* arrow in a). The positive skewed distribution of the increments points out the asymmetry of the rolls observed in a). In this example, backscatter coefficient increases when leaving rolls are sharper than decreases when entering into the rolls which leads to larger values of positive increments than those of negative ones and so to a positive skewed distribution of the increments.

## 3. Datasets

### 3.1. *Sentinel-1 SAR Wave Mode dataset*

Nowadays, the largest database of C-band Synthetic Aperture Radar (SAR) images of the ocean is provided by the Sentinel-1 constellation mission. Sentinel-1A and Sentinel-1B twin SAR can operate in 4 different and exclusive acquisition modes. They differ in incidence angle range, swath width (spatial coverage), resolution and polarization. In this work we focus on the WV acquisition mode, which provides images of 20 km $\times$ 20 km (the smallest) with a spatial resolution of 5 m (the highest). Then, this mode furnishes large enough images to study convective rolls (typical wavelengths of 2-20 km), while covering quite homogeneous areas and at very high spatial resolutions.

We work on previously preprocessed Sentinel-1 SAR WV images from https://xwaves.ifremer.fr/#/ (Wang et al. 2020). These images are corrected from the mean decrease (due to local incidence angle change across the image) of the backscattered signal measured by SAR for a scene assumed homogeneous and present a final spatial resolution after preprocessing of 50 m which allows us to study convective rolls but also events with smaller wavelengths such as swell (typically 200 m; up to 800 m). To illustrate the potential impact of swell on the OLE signature in SAR images, we study here two different images: both obtained by Sentinel-1 A, one between 11:30:04 and 11:30:07 on 15 March 2017 from Great Lakes in the border between U.S.A and Canada and another between 20:25:22 and 20:25:24 on 29 December 2016 from open North Pacific ocean. While the last one presents a significant swell event, the first one is free of this phenomena, see Fig. 2. These study cases have been chosen to illustrate

the power and limitations of the proposed methodology to characterize convective rolls from SAR images. Moreover, the analysis of many other Sentinel-1 SAR images containing rolls supports the results and conclusions presented in next sections.

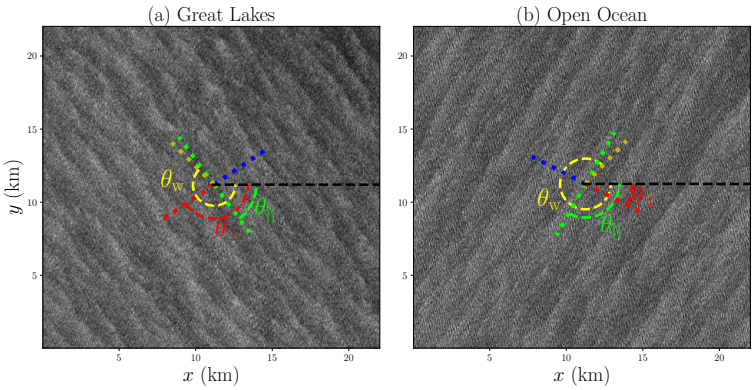


**Figure 2.** Sentinel-1 SAR images of the ocean: left Great Lakes and right North Pacific. Green dashed lines correspond to the parallel ($\theta_{||}$) and blue and red dashed lines to the perpendicular ($\theta_{\perp}$) directions of convective rolls as obtained from $S_2^{l_x,l_y}$. Red indicates the direction with positive skewness and blue with negative one. Yellow dashed line indicates the wind direction ($\theta_{\mathrm{w}}$) obtained from ECMWF global model.

### 3.2. *HRES wind direction from ECMWF global model*

HRES (High RESolution Forecast) is the highest-resolution operational model at global scale of the European Center for Medium-Range Weather Forecasts (ECMWF). It provides several environmental variables hourly and on a global spatial grid of 0.1° by 0.1°. Here, we focus on the meridional and zonal wind component at 10-m height from atmospheric model high resolution 10-day forecast (Set I - HRES) to compute wind direction. The data are publicly available at https://www.ecmwf.int/en/forecasts/datasets/set-i. In this study we rely on the closest forecast in time to compare with the measurements.

## 4. Results and discussion

### 4.1. *Second-order structure functions*

Fig. 3 shows $S_2^{l_x,l_y}$ and $S_2^{r,\theta}$ for the Great Lakes and the North Pacific Ocean SAR images presented in section 3.1. For both SAR images, we observe a ellipsoidal structure of a given width about 1 km (green dashed vertical line in polar coordinates) and with its long axis along a given direction $\theta_{||}$ (horizontal green dashed line in polar coordinates). Thus, the second order structure function applied on SAR images characterizes the wavelength and direction of convective rolls, see table 1. Same results were obtained with power spectrum (Wang et al. 2019, 2020) and correlation (Lohou, Druilhet, and Campistron 1998) methodologies. Moreover, the swell — if present — can be characterized in the same way, but looking at smaller scales (see Fig. 3 b). Its presence is revealed by ellipsoidal structures of $S_2^{l_x,l_y}$ at small scales (inside the black square in Fig. 3 b). The direction and wavelength of the swell is also obtained (and represented as black dashed lines in Fig. 3 d). We obtain a swell wavelength of 120 m in agreement with the WaveWatch3 model (130 m) and Fourier analysis (118 m).

However, the resolution of our measures is the pixel size, here 50 m, and so swell scales are too small for our method to be adapted.

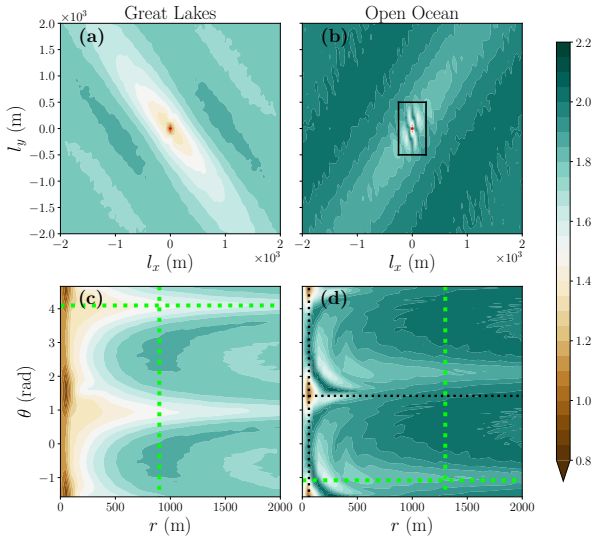


**Figure 3.** Two-dimensional second-order structure function of two Sentinel-1 SAR images of the ocean: left Great Lakes and right North Pacific. Top in cartesian coordinates $S_2^{l_x,l_y}$, bottom in polar coordinates $S_2^{r,\theta}$. In a) and b) the center $l_x = l_y = 0$ is indicated with a red dot. In figure b) a black square has been added to point out the signature of the swell. In figures c) and d) horizontal and vertical green dashed lines indicate respectively the direction and wavelength of convective rolls. In figure d) black dashed lines indicate the direction and wavelength of swell.

**Table 1.** Wavelength and direction of convective rolls from Great Lakes and Open ocean SAR images as obtained from $S_2^{r,\theta}$.

| | **Great Lakes** | **Open Ocean** |
|---|---|---|
| $\theta_{\|\|}$ (rad) | 0.95 $(0.95 - \pi)$ | 2.06 $(2.06 - \pi)$ |
| $\theta_\perp$ (rad) | $0.95 \pm \pi/2$ | $2.06 \pm \pi/2$ |
| Wavelength (m) | 1800 | 2600 |

### 4.2. *Third-order structure functions*

Fig. 4 shows $\mathcal{S}^{l_x,l_y}$ and $\mathcal{S}^{r,\theta}$ for the two SAR images. Whereas the line parallel to the direction of the rolls $\theta_{||}$ passing by the center was a symmetry line for $S_2^{l_x,l_y}$, it is now an anti-symmetry line for the skewness $\mathcal{S}^{l_x,l_y}$, because $\mathcal{S}^{l_x,l_y}$ is now an odd function of $(l_x, l_y)$: $\mathcal{S}^{l_x,l_y} = -\mathcal{S}^{-l_x,-l_y}$.

For both SAR images, Fig. 4 shows that along $\theta_{||}$ there is no asymmetry, while along the direction perpendicular to the rolls, $\theta_\perp$, $\mathcal{S}^{l_x,l_y} \neq 0$ for scales smaller than the rolls scale, and so rolls are asymmetrical along this direction, *i.e.* rises and falls of the field are not symmetrical. Furthermore, along $\theta_\perp$ for scales larger than the roll scales $\mathcal{S}^{l_x,l_y} \approx 0$. Finally, for both images wind direction presents a positive skewness (see yellow lines in Fig. 4 and Fig.2), pointing out a possible impact of wind direction on the rolls asymmetry.

In Fig. 4 a) strong negative values of $\mathcal{S}^{l_x,l_y}$ are observed when going through $\theta_\perp = -0.62$ rad. This direction corresponds to the blue dashed line in figure 2 a). Thus

$\mathcal{S}^{l_x,l_y} < 0$ at scales smaller than the rolls scale and goes to 0 once this scale is reached. This implies an asymmetry in rolls shape along their perpendicular direction. More precisely, along $\theta_\perp = -0.62$ rad SAR intensity falls are sharpener than rises and so, we leave rolls more smoothly than we enter into them. This asymmetry is also observed in $\mathcal{S}^{r,\theta}$, Fig. 4 c).

In Fig. 4 b) and d) negative skewness along $\theta_\perp = 3.63$ rad indicates also an asymmetry in rolls shape along this direction which corresponds to the blue dashed line in figure 2 b). Along this direction we enter into rolls more sharply than we leave them. Moreover, the swell presence in the SAR image from open ocean adds a small scale effect into the analysis of high-order statistics since swell presents also asymmetries which are characterized by the skewness.

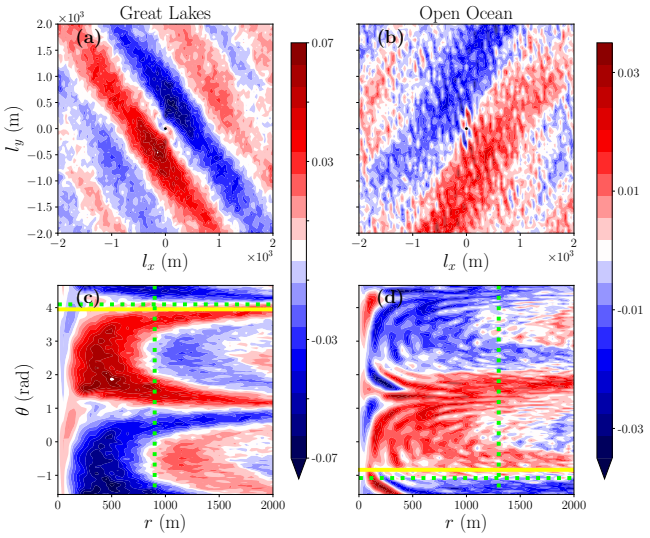


**Figure 4.** Two-dimensional skewness across scales of two Sentinel-1 SAR images of the ocean: left Great Lakes and right North Pacific. Top in cartesian coordinates $\mathcal{S}^{l_x,l_y}$, bottom in polar coordinates $\mathcal{S}^{r,\theta}$. In a) and b) the center $l_x = l_y = 0$ is indicated with a black dot. In figures c) and d) horizontal and vertical green dashed lines indicate respectively the direction and wavelength of convective rolls and the horizontal yellow line indicates the wind direction from ECMWF global model.

### 4.3. *Fourth-order structure functions*

Fig. 5 shows $\mathcal{F}^{l_x,l_y}/3$ and $\mathcal{F}^{r,\theta}/3$ for different scales and directions. We observe ellipsoidal structures from which the direction and shape of rolls can be obtained, especially for the Great Lakes case without swell, while for the open ocean case the observation is more blurry. The evolution of $\mathcal{F}^{r,\theta_\perp}/3$ across scales indicates the intermittent nature of the rolls evolution along this direction. On the contrary, $\mathcal{F}^{r,\theta_{||}}/3$ seems to remain constant. Finally, the obtained values of the flatness are slightly larger than those of a Gaussian distribution, so implying increment distributions with larger tails than Gaussian.

### 4.4. *Transects*

Fig. 6 shows $\theta$-transects of $S_2^{r,\theta}$, $\mathcal{S}^{r,\theta}$ and $\mathcal{F}^{r,\theta}/3$ as a function of $r$ for both studied SAR images. Gray lines correspond to all the studied directions $\theta$, while the direction

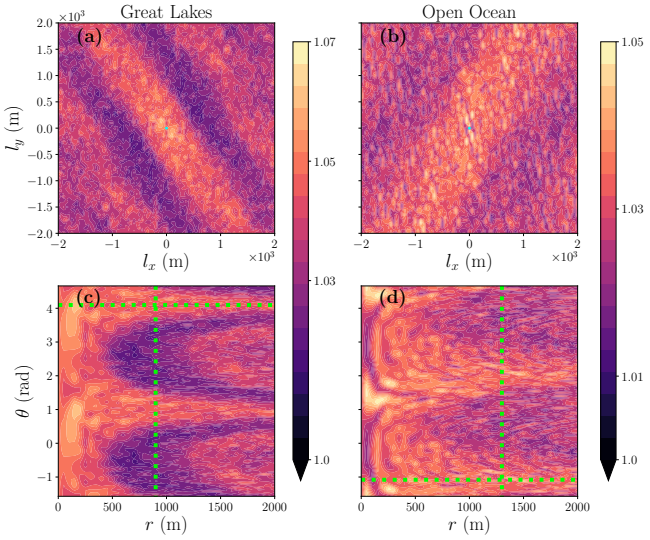


**Figure 5.** Two-dimensional flatness across scales of two Sentinel-1 SAR images of the ocean: left Great Lakes and right North Pacific. Top in cartesian coordinates $\mathcal{F}^{l_x,l_y}/3$, bottom in polar coordinates $\mathcal{F}^{r,\theta}/3$. In a) and b) the center $l_x = l_y = 0$ is indicated with a cyan dot. In figures c) and d) horizontal and vertical green dashed lines indicate respectively the direction and wavelength of convective rolls.

parallel to the rolls is highlighted in green circles and the directions perpendicular to the rolls are highlighted in red and blue asterisks. We focus then on $\theta_\perp$ and $\theta_{||}$ since they show up the more extreme behaviors with all the other directions in between.

In Fig. 6 a) and b) $S_2^{r,\theta}$ increases from small values at small scale to a higher value plateau at large scale. This plateau is reached faster in the perpendicular direction than along the parallel direction.

Fig. 6 c) and d) show $\mathcal{S}^{r,\theta}$ which evolves very differently depending on $\theta$. Along $\theta_{||}$ $\mathcal{S}^{r,\theta_{||}}$ remains constant and equal to zero. On the contrary, along $\theta_\perp$ it is different than zero for scales smaller than the rolls scales and go back to zero for scales larger than the rolls scale. Each perpendicular direction correspond to a different sign of the skewness due to the inverse symmetry explained above. In the case of Great lakes, where swell is not present, $\mathcal{S}^{r,\theta_\perp}$ shows the maximum/minimum values. In the case of the open ocean image this is less clear due to the noise induced by the swell.

Finally, Fig. 6 e) and f) show the evolution of $\mathcal{F}^{r,\theta}/3$ for both studied images. On the one hand, for Great Lakes $\mathcal{F}^{r,\theta_{||}}/3$ is almost constant at a value close to 1.05, indicating a distribution slightly more tailed than a Gaussian. On the contrary, $\mathcal{F}^{r,\theta_\perp}/3$ decreases and approaches 1 at scales smaller than the rolls scale. Then at large scales, it turns up to the $\mathcal{F}^{r,\theta_{||}}/3$ value. This evolution of $\mathcal{F}^{r,\theta_\perp}/3$ across scales is a signature of intermittency. On the other hand, for open ocean $\mathcal{F}^{r,\theta}/3$ seems to be constant for all directions being impossible to discriminate between $\theta_{||}$ and $\theta_\perp$. This can be newly due to the swell that difficult the analysis.

## 5. Conclusions

We proposed second and higher order structure functions to analyse the morphology of convective rolls through the study of Sentinel-1 SAR images of the ocean. We chose two different study cases: one image in the Great Lakes and the other in the North Pacific, to illustrate the characterization of rolls provided by the proposed methodol-

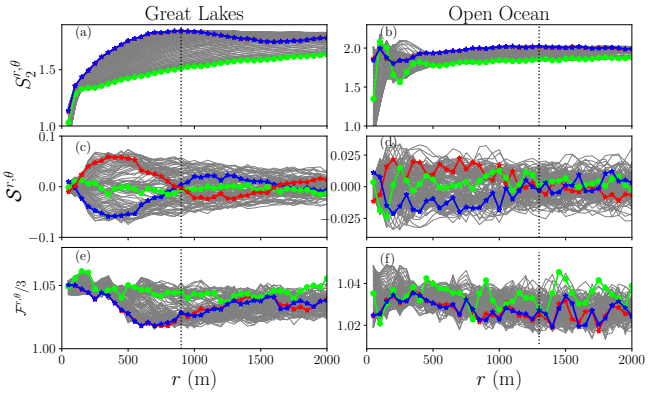


**Figure 6.** One-dimensional $\theta$-transects of $S_2^{r,\theta}$ (a and b), $\mathcal{S}^{r,\theta}$ (c and d) and $\mathcal{F}^{r,\theta}/3$ (e and f) as a function of $r$ for two Sentinel-1 SAR images of the ocean: left Great Lakes and right Open ocean. Direction $\theta_{||}$ is highlighted in green dots and directions $\theta_\perp$ and $\theta_\perp + \pi$ are highlighted in blue and red asterisks respectively. Vertical black dashed line correspond to the maximum value of $S_2^{r,\theta}$ which is used to define the wavelength of the roll.

ogy. Moreover, we have studied several tens of Sentinel 1 SAR images obtaining the same qualitative results.

Thus, we showed that $S_2^{l_x,l_y}$ characterizes the direction and wavelength of convective rolls, just like correlation (Lohou, Druilhet, and Campistron 1998) or power spectrum (Wang et al. 2019, 2020) do. Moreover, and contrary to correlation and power spectrum, structure functions can be easily generalized ($\mathcal{S}^{l_x,l_y}$ and $\mathcal{F}^{l_x,l_y}/3$) to grasp high-order statistics and so to provide finer information on the shape of convective rolls. While $\mathcal{S}^{l_x,l_y}$ characterized the asymmetry of convective rolls along the direction perpendicular to the rolls $\theta_\perp$, $\mathcal{F}^{l_x,l_y}/3$ pointed out the intermittent nature of convective rolls also along $\theta_\perp$. This is the first time that both the rolls asymmetry and intermittency, and consequently their turbulent nature, is described from the analysis of SAR images of the ocean.

In open ocean and on SAR images at 50 m resolution, swell can hinder the analysis of high order statistics due to the small scale fluctuations that it produces on the measures. However, preliminary analysis show than a low-pass filtering (or equivalently working on pre-processed SAR images at 200 m) could filter out the swell signature. Such a filtering may require specific analysis to be adjusted depending on waves properties (e.g. swell orientation with respect to wind direction, swell wavelength *etc*)

Future research will deal with better understanding the relationship between rolls asymmetry and atmospheric conditions such as wind direction or shear intensity. Finally, the codes used in this article to estimate two-dimensional structure functions are provided at: https://github.com/cgranerob/2D-Structure-Functions.

## Funding

This work was supported by the French National Research Agency (ANR-21-CE46-0011-01).

## References

Alpers, W., and B. Brümmer. 1994. "Atmospheric boundary layer rolls observed by the synthetic aperture radar aboard the ERS-1 satellite." *Journal of Geophysical Research* 99 (C6):

12613. https://doi.org/10.1029/94JC00421.

Atta, C. W. Van, and W. Y. Chen. 1970. "Structure functions of turbulence in the atmospheric boundary layer over the ocean." *Journal of Fluid Mechanics* 44 (1): 145–159. https://doi.org/10.1017/S002211207000174X.

Babin, S. M., T. D. Sikora, and N. S. Winstead. 2003. "A case study of satellite synthetic aperture radar signatures of spatially evolving atmospheric convection over the Western Atlantic Ocean." *Boundary-Layer Meteorology* 106: 527–546. https://doi.org/10.1023/A:1021236600569.

Etling, D., and R. A. Brown. 1993. "Roll vortices in the planetary boundary layer: A review." *Boundary-Layer Meteorology* 522 (65): 215–248. https://doi.org/10.1007/BF00705527.

Frisch, U. 1995. *Turbulence: the legacy of A.N. Kolmogorov*. Cambridge University Press. https://doi.org/10.1017/CBO9781139170666.

Kolmogorov, A. N. 1962. "A refinement of previous hypotheses concerning the local structure of turbulence in a viscous incompressible fluid at high Reynolds number." *Journal of Fluid Mechanics* 13: 82–85. https://doi.org/10.1017/S0022112062000518.

Lohou, F., A. Druilhet, and B. Campistron. 1998. "Spatial and temporal characteristics of horizontal rolls and cells in the atmospheric boundary layer based on radar and in situ observations." *Boundary-Layer Meteorology* 89: 407–444. https://doi.org/10.1023/A:1001791408470.

Obukhov, A. M. 1962. "Some specific features of atmospheric turbulence." *Journal of Fluid Mechanics* 13: 77–81. https://doi.org/10.1017/S0022112062000506.

Saggiorato, B., L. Nuijens, A. P. Siebesma, S. de Roode, I. Sandu, and L. Papritz. 2020. "The influence of convective momentum transport and vertical wind shear on the evolution of a cold air outbreak." *Journal of Advances in Modeling Earth Systems* 12: e2019MS001991. https://doi.org/10.1029/2019MS001991.

Sandu, I., A. Beljaars, P. Bechtold, T. Mauritsen, and G. Balsamo. 2013. "Why is it so difficult to represent stably stratified conditions in numerical weather prediction (NWP) models?" *Journal of Advances in Modeling Earth Systems* 5: 117–133. https://doi.org/10.1002/jame.20013.

Sikora, T. D., and S. Ufermann. 2004. *SAR Users Manual*, Chap. 14. Marine Atmospheric Boundary Layer Cellular Convection and Longitudinal Roll Vortices, 321–330. National Oceanic and Atmospheric Administration, U.S. Department of Commerce. https://www.sarusersmanual.com/.

Tandeo, P., E. Autret, B. Chapron, R. Fablet, and R. Garello. 2014. "SST spatial anisotropic covariances from METOP-AVHRR data." *Remote Sensing of Environment* 141 (5): 144–148. https://doi.org/10.1016/j.rse.2013.10.024.

Wang, C., A. Mouche, R. C. Foster, D. Vandemark, J. E. Stopa, P. Tandeo, N. Longepe, and B. Chapron. 2019. "Characteristics of Marine Atmospheric Boundary Layer roll vortices from Sentinel-1 SAR Wave Mode." In *IGARSS 2019 - 2019 IEEE International Geoscience and Remote Sensing Symposium*, doi:10.1109/IGARSS.2019.8900287.

Wang, C., D. Vandemark, A. Mouche, B. Chapron, H. Li, and R. C. Foster. 2020. "An assessment of marine atmospheric boundary layer roll detection using Sentinel-1 SAR data." *Remote Sensing of Environment* 250: 112031. https://doi.org/10.1016/j.rse.2020.112031.

Young, G. S., D. A. R. Kristovich, M. R. Hjelmfelt, and R. C. Foster. 2002. "Rolls, streets, waves, and more: A review of quasi-two-dimensional structures in the atmospheric boundary layer." *Bulletin of the American Meteorological Society* 83: 997–1001. http://dx.doi.org/10.1175/BAMS-83-7-Young.

Zhang, J. A., K. B. Katsaros, P. G. Black, S. Lehner, J. R. French, and W. M. Drennan. 2008. "Effects of roll vortices on turbulent fluxes in the hurricane boundary layer." *Boundary-Layer Meteorology* 128: 173–189. https://doi.org/10.1007/s10546-008-9281-2.